Essential Readings in Light Metals: Cast Shop for Aluminum Production.
Edited by John F. Grandfield and Dmitry G. Eskin.

THE MECHANISM OF PULL-IN DURING DC-CASTING OF ALUMINIUM SHEET INGOTS

Hallvard G. Fjær
Institute for Energy Technology
P.O. Box 40 N-2007 Kjeller, Norway

Arild Håkonsen
Hydro Aluminium R&D Materials Technology
P.O. Box 219 N-6601 Sunndalsøra, Norway

Abstract

The pull-in phenomenon apparent in the DC-casting process of aluminium sheet ingots is investigated both analytically and by use of numerical models calculating temperatures, strains and stresses. The major part of the pull-in takes place above the bottom of the sump, but is mainly caused by thermal contractions and deformations in regions below.

The strong and almost exactly linear dependency of the pull-in on the casting speed is explained. The effects on the pull-in of different cooling conditions and of various thermophysical and thermomechanical properties are investigated.

A 2D plain strain approximation has been successfully applied in calculating the pull-in for the centre part of the rolling face, but 3D effects are significant close to the narrow ingot surface. This is illustrated by comparison of results from 3D and 2D calculations. Modelling results are also compared with measurements of ingot thickness variations, and a good agreement is obtained.

Introduction

In D.C. casting of aluminium sheet ingots, thermomechanical effects due to varying cooling rates and corresponding thermal contractions induce geometrical distortions of the final ingot shape. If a rectangular mould is applied, the ingot will obtain a concave or "bone shaped" cross section profile at stationary casting conditions. This is due to the pull-in, or inward contractions which are excessive at the central regions of the rolling faces. At the bottom of the ingot, and near the narrow ingot sides, the difference between the final ingot thickness and the mould opening corresponds to the thermal contraction associated with the cooling from the solidification temperature to the room temperature. As stationary casting conditions are approached, a gradually increasing effect of the pull-in leads to the thickness decreasing with casting length at the central regions of the rolling faces. This is commonly denoted as the "butt swell". These geometrical effects are illustrated in Figure 1. Efforts are made to minimize the deviations from flat rolling faces, as such deviations may require expensive scalping of the ingot. Concave mould openings are commonly applied to compensate for the pull-in [1,2]. The butt swell has been reported to be reduced or eliminated by the use of an insulated pad on the top of the centre area of the starting block [3], or by application of a flexible mould [4]. The starting block shape may also have an impact on the butt swell profile [5]. The pull-in is dependent on the ingot dimensions, the casting parameters and the thermal and mechanical properties of the actual alloy. An empirical model relating the pull-in to the casting speed, thickness and alloy has been developed by Weaver et al. [2]. In a paper by Håkonsen [6], closely related to this work, an explicit formula for the mould opening profile leading to flat rolling faces is proposed. Thermally induced deformations of sheet ingots, such as pull-in, can be calculated by numerical models solving the equations for conservation of energy, mass and momentum. Measurements and numerical predictions of the pull-in for aluminium sheet ingots have been the major topics of a recent work by Drezet [7,8,9,10].

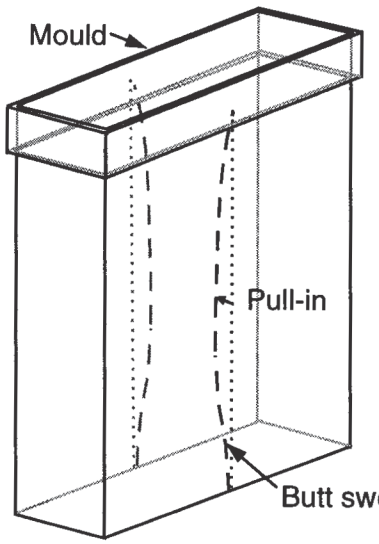

Figure 1: DC-casting of a sheet ingot in a rectangular mould. The pull-in and the butt swell are illustrated

The main purpose of this paper is to explain two observations concerning the pull-in phenomenon. One is the strong and almost exactly linear dependency of the pull-in on the casting speed. The second is the fact that the pull-in is nearly independent of alloy composition [6,8]. This observation is a bit surprising considering the significant differences in the material properties of the various alloys. In order to explain these phenomena the pull-in mechanism is investigated both analytically and numerically. First an analytical expression for the pull-in is derived based on a series of assumptions and approximations concerning the DC-casting process and the governing equations. Next the thermal 3D model

ALSIM3 [11] and the mechanical 3D model ALSPEN3 [12,13] are applied in numerical simulations of the DC-casting process. The calculated pull-in is compared with measurements for ingots of the alloys AA1050 and AA3003. The potentials and limitations of much faster 2D simulations are discussed and 2D results are compared with 3D results. Finally, 2D simulations are used in parameter studies concerning casting conditions and material properties, and numerical results are compared with results derived analytically.

Analytical expressions

Weaver [1] found the following relation between the mould opening D_M, the final ingot thickness D, and the casting velocity V to be valid for a wide range of dimensions and casting speeds, provided the width to thickness ratio is sufficiently large:

$$D_M = C_1 D + C_2 D^2 V \tag{1}$$

Here, C_1 accounts for the (small) reduction in thickness below the bottom of the sump due to thermal contractions, and C_2 is a constant considered to be alloy dependent [2]. The second term of the right hand side of (1) normally accounts for about 90% of the total pull-in, defined as half of the total reduction of ingot thickness, i.e. $(D_M - D)/2$. This simple dependency of the pull-in on the casting speed for a given dimension could be expected to have a simple explanation. However, the mechanism of pull-in, identified as a bending of the solid shell induced by horizontal thermal gradients [7,10], has to our knowledge only been described qualitatively.

Through applying dimensional analysis, and a series of approximations and simplifications concerning the boundary conditions and the material properties, we will attempt to uncover the basic mechanism of the pull-in and to identify the most important parameters involved. We consider stationary casting conditions and focus on one half of a semi-infinite cross section at the centre of the wide ingot side. We apply an Eulerian frame of reference where the origin is positioned at the top of the solidified region. The domains Ω_1 and Ω_2, i.e. the regions above and below the bottom of the sump (see Figure 2), are treated separately.

The temperature field

As the pull-in is generated by thermal contractions, we first have to obtain an expression for the temperature field $T(y,z)$. We neglect the heat diffusion in the x-direction (normal to our 2D solution domain) and any fluid flow differing from the casting velocity V, and we assume temperature independent thermal conductivity λ, density ρ, specific heat capacity c_p, and resulting thermal diffusivity $\alpha = \lambda/(\rho\, c_p)$. Let ΔH_m be the latent heat of solidification and f_s the solid fraction. The conservation of energy can then be expressed by:

$$\lambda\frac{\partial^2 T}{\partial y^2} + \lambda\frac{\partial^2 T}{\partial z^2} = V\rho\left(c_p + \Delta H_m \frac{\partial f_s}{\partial T}\right)\frac{\partial T}{\partial z} \tag{2}$$

Introducing $\Phi = 1 + \dfrac{\Delta H_m}{c_p}\dfrac{\partial f_s}{\partial T}$ from [14], the Peclet number

$$\mathrm{Pe} = \frac{VD}{\alpha} = \frac{VD\rho c_p}{\lambda} \quad , \tag{3}$$

and the dimensionless coordinates $Y=y/D$ and $Z=z/D$ gives:

$$\frac{\partial^2 T}{\partial Y^2} + \frac{\partial^2 T}{\partial Z^2} = \mathrm{Pe}\,\Phi\frac{\partial T}{\partial Z} \tag{4}$$

The Peclet number Pe may be interpreted as the relative importance of heat convection to heat diffusion in the casting direction. In the case of DC-casting of sheet ingots, the Peclet number is normally in the range of 7 to 15, hence heat diffusion in the Z-direction can be considered to be of minor importance [14]. Omitting this term we obtain:

$$\frac{\partial^2 T}{\partial Y^2} = \mathrm{Pe}\,\Phi\frac{\partial T}{\partial Z} \tag{5}$$

From (5) we see that the temperature field expressed as a function of dimensionless coordinates is dependent on the Peclet number only. We will in the following use dimensional quantities. More generalized expressions can easily be obtained by inserting variables for dimensionless velocities, lengths and temperatures.

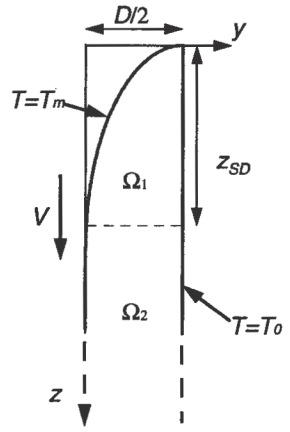

Figure 2. Solution domain, axes of reference and boundary conditions for the analytical solution of the pull-in.

The surface temperature is taken to have a constant value T_0 along the whole cooling surface. This is close to reality for large ingots, but any effect of the primary cooling is consequently neglected. We consider a pure metal entering with a temperature equal to the melting temperature T_m. With these approximations, there exists a known analytical solution of (5), see e.g. [15]. The position of the solidification front y_M is then in our chosen frame of reference

$$y_M = \frac{D}{2} - 2\eta\sqrt{\frac{\alpha z}{V}} = \frac{D}{2} - 2\eta\sqrt{\frac{zD}{\mathrm{Pe}}} \quad , \tag{6}$$

where η is the root of the equation:

$$\eta\exp(\eta^2)\,\mathrm{erf}(\eta) = \mathrm{St}/\sqrt{\pi} \tag{7}$$

η is only dependent on the Stefan number St, defined by the ratio of the latent heat of cooling to the latent heat of solidification:

$$\mathrm{St} = c_p(T_m - T_0)/\Delta H_m \tag{8}$$

From (6) the sump depth z_{SD} may be expressed as:

$$z_{SD} = \frac{D^2 V}{16\eta^2\alpha} = \frac{D\,\mathrm{Pe}}{16\eta^2} \tag{9}$$

In the domain Ω_2 the solution of (5) may be written as

$$T(y,z) = T_0 + (T_m - T_0) \cdot \sum_{n=0}^{\infty} c_n \exp\left(-(2n+1)^2 \frac{\pi^2}{\mathrm{Pe}} \frac{z+z_{SD}}{D}\right) \cos\left((2n+1)\pi \frac{y}{D}\right) \quad (10)$$

where the coefficients c_n depend on the boundary conditions on the top of the domain. We disregard all but the first term of the series in (10), and we linearize the dependency of T on y. This finally gives:

$$T(y,z) = T_0 + (T_m - T_0)\left(1 - \frac{2y}{D}\right)\sqrt{\frac{z_{SD}}{z}} \quad \text{in } \Omega_1 \quad (11)$$

$$T(y,z) = T_0 + (T_m - T_0)\left(1 - \frac{2y}{D}\right)\exp\left(-\frac{\pi^2}{\mathrm{Pe}} \frac{z - z_{SD}}{D}\right) \quad \text{in } \Omega_2 \quad (12)$$

The velocity field

Next, we will derive expressions for the components v_y and v_z of the velocity field where the nominal casting speed V has been subtracted. We consider plane strain ($\partial v_x/\partial x = 0$), although this assumption is only correct for an ingot of infinite width. We also assume a temperature independent thermal linear expansion coefficient β, and consider the material to be incompressible. Then continuity requires:

$$\frac{\partial v_y}{\partial y} + \frac{\partial v_z}{\partial z} = 3\beta V \frac{\partial T}{\partial z} \quad (13)$$

The domain Ω_1 can freely bend inwards, but the domain Ω_2 is constrained by the symmetry condition v_y=0 at y=0. This induces deformations. We consider the three modes of deformation illustrated by their associated velocity fields in Figure 3 to be the most important.

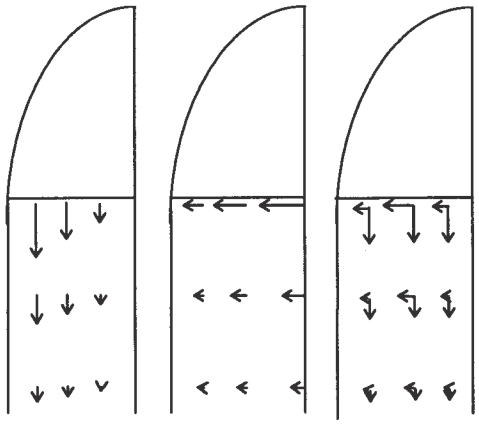

Figure 3: Velocity fields in domain Ω_2 associated with three different deformation modes compatible with the thermal contractions.

In mode I, all thermal contractions are compensated for by an additional vertical velocity. This mode entails no reduction of ingot thickness in domain Ω_2, but it induces an inward bending of the domain Ω_1 associated with the angular velocity $\dot{\omega} = \partial v_z/\partial y$ at the boundary between the domains. Mode II involves only horizontal velocities, and represents a maximum reduction of ingot thickness in domain Ω_2. The nonzero horizontal velocity at the top of domain Ω_2 at y=D/2 represents an "inward pulling" of the domain Ω_1. In mode III the vertical velocity is constant over a horizontal cross section, whereas the v_y component have a parabolic variation with a zero value at the cooling surface. This mode does not entail any reduction of the ingot thickness, but it involves a compression of the coldest part of the ingot having the largest flow stress. Results from numerical simulations indicate that mode III is of rather low relative importance for casting of aluminium alloys. In order to keep the algebraic expressions simple, we choose to disregard this deformation mode in what follows. However, in a more extensive analysis this mode should be included.

Assuming weight factors r for mode I and $(1\text{-}r)$ for mode II, we may express the velocity field in domain Ω_2 as:

$$v_y = -3(1-r)\beta V(T_m - T_0)\frac{\pi^2}{\mathrm{Pe}\,D}\left(y - \frac{y^2}{D}\right)\exp\left(-\frac{\pi^2}{\mathrm{Pe}} \frac{z - z_{SD}}{D}\right) \quad (14)$$

$$v_z = 3r\beta V(T_m - T_0)(1 - \frac{2y}{D})\exp\left(-\frac{\pi^2}{\mathrm{Pe}} \frac{z - z_{SD}}{D}\right) \quad (15)$$

The domain Ω_1 is considered to be in a state of uniaxial tension in the x-direction induced by the plane strain condition. Let $\dot{\varepsilon}_{ij}^{th}$ and $\dot{\varepsilon}_{ij}$ denote components of the thermal and total strain rate tensor, respectively. The following velocity field can be seen to be compatible with a von Mises viscoplastic flow, i.e. $\dot{\varepsilon}_{yy} = \dot{\varepsilon}_{zz} = \frac{1}{2}\dot{\varepsilon}_{ii}^{th}$ (sum over indices), and a zero shear strain rate at the cooling surface of Ω_1:

$$v_y = -3\beta V(T_m - T_0)\left[\frac{1}{4}\sqrt{\frac{z_{SD}}{z^3}}\left(-\frac{y^2}{D} + y - \frac{D}{4}\right) + \frac{2}{D}\left(\left(\frac{1}{2} - r\right)(z - z_{SD}) + z_{SD} - \sqrt{z_{SD}z}\right) + \frac{\pi^2}{4\,\mathrm{Pe}}(1-r)\right] \quad (16)$$

$$v_z = \frac{3}{2}\beta V(T_m - T_0)\left(1 - \frac{2y}{D}\right)\left(\sqrt{\frac{z_{SD}}{z}} + 2r - 1\right) \quad (17)$$

The velocity component v_z is continuous at the domain boundary, i.e. at z=z_{SD}, but the v_y velocity component is discontinuous, corresponding to a localized shear strain rate, except for y=D/2. The factor r is at this point the only unknown. If we apply a linear and temperature independent constitutive law of the type $\bar{\sigma} = A\dot{\bar{\varepsilon}}$ or $\bar{\sigma} = A\bar{\varepsilon}$, where $\bar{\sigma}$, $\bar{\varepsilon}$ and $\dot{\bar{\varepsilon}}$ are the effective values of stress, strain and strain rate, it can be shown that the following value of r minimizes the integrals associated with elastic energy or energy dissipation, ($\frac{1}{2}\int_{\Omega_2} \bar{\sigma}\bar{\varepsilon}\,dy\,dz$ and $\frac{1}{2}\int_{\Omega_2} \bar{\sigma}\dot{\bar{\varepsilon}}\,dy\,dz$):

$$r = \frac{1 + 30\frac{\mathrm{Pe}^2}{\pi^4}}{1 + 60\frac{\mathrm{Pe}^2}{\pi^4} + 120\frac{\mathrm{Pe}^4}{\pi^8}} \quad (18)$$

The derivation of (18) involves some elaborate algebra, and such expressions easily become prone to errors. However, by use of the interactive computer algebra system Maple[1] [16] reliable results were more easily obtained.

[1] Maple is a registred trademark of Waterloo Maple Software

The pull-in

By integrating (14) and (16) the horizontal displacement u_y at the cooling surface of Ω_1 can be expressed as:

$$u_y = -3\beta(T_m - T_0)\cdot \left[\left(\frac{1}{2}-r\right)\frac{z^2}{D}+(1+2r)\frac{\mathrm{Pe}}{16\eta^2}z-\frac{1}{3\eta}\sqrt{\frac{\mathrm{Pe}}{D}z^3}+\frac{\pi^2}{4\,\mathrm{Pe}}(1-r)z\right] \quad (19)$$

The corresponding displacement at the surface of Ω_2 becomes:

$$u_y = -3\beta(T_m - T_0)D\left(\frac{\mathrm{Pe}^2}{256\eta^4}\left(\frac{1}{6}+r\right)+(1-r)\left\{\frac{\pi^2}{64\eta^2}+\frac{1}{4}\left[1-\exp\left(-\frac{\pi^2}{\mathrm{Pe}}\frac{z-z_{SD}}{D}\right)\right]\right\}\right) \quad (20)$$

The relative pull-in after casting can then be expressed by:

$$\frac{-u_{y,(z\to\infty)}}{D/2} = 3\beta(T_m - T_0)\cdot \left[\frac{\mathrm{Pe}^2}{768\eta^4}+\frac{\mathrm{Pe}^2}{128\eta^4}r+(1-r)\frac{\pi^2}{32\eta^2}+\frac{(1-r)}{2}\right] \quad (21)$$

Each of the four terms in (21) can be given a specific physical interpretation. The first term represents the pull-in in the domain Ω_1 caused by thermal contractions within this domain. The second and third term are respectively the effect of bending/tilting and horizontal pulling of the domain Ω_1 caused by deformations in the domain Ω_2. The last term represents the reduction of ingot thickness in the domain Ω_2. It should be noted that the expressions inside the square brackets in (21) are only dependent on the Peclet number and the Stefan number, as r is only dependent on Pe, and η is only dependent on St. In Figure 4 the analytically predicted pull-in, based on the thermophysical data from Table I is compared with literature data from Weaver [1]. A very good agreement is obtained. Eq. (1) can be rewritten to express the relative pull-in as a constant term plus a linear function of the Peclet number.

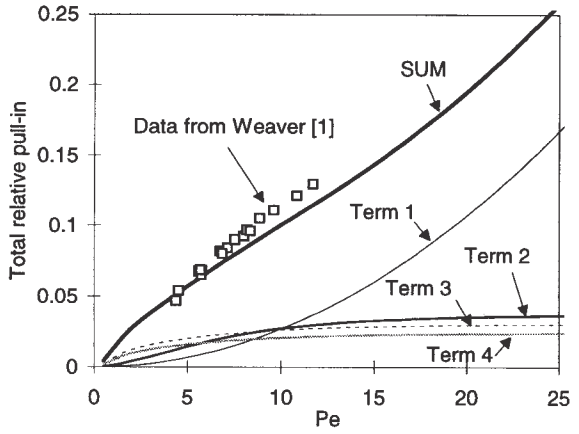

Figure 4: The relative pull-in of DC cast AA1050 ingots as a function of Peclet number. Approximative analytical solution compared with data from literature.

This figure also shows the importance of each of the four terms in eq. (21). Within the range of Peclet numbers relevant for DC casting, all four terms are of significant importance. The 4th term is presumably somewhat overestimated, due to the plane strain approximation and the omission of the deformation mode III. Surprisingly, (21) contains no explicit linear term of the Peclet number. This is also the situation if (18) is inserted. However, the second derivative of the right hand side of (21) with respect to Pe is zero for a value of Pe close to 10, leading to a linear appearance. The first term in (21) increase quadratically with Pe whereas the three other terms converge to their limit values as r approaches zero for very large Peclet numbers. According to (18), the strain rate field in the domain Ω_2 should appear quite differently for low and high Peclet numbers. For very large Peclet numbers, the first term in (21) should be the dominating one leading to a more nonlinear relationship between the pull-in and the Peclet number. These predictions will be checked by numerical simulations in a later section.

Table I: Thermophysical data for AA1050 and environment temperature applied in analytical solution of pull-in.

Property	Unit	Value	Property	Unit	Value
λ	[W/m K]	215	β	[1/K]	$30\cdot10^{-6}$
ρ	[kg/m^3]	2705	T_m	[°C]	650
c_p	[J/kg K]	1000	T_0	[°C]	100
ΔH_m	[J/kg]	400000			

Thermal modelling

In two reference cases DC casting of 1500 mm × 600 mm sheet ingots of the alloys AA1050 and AA3003 were simulated by using the 3D thermal model ALSIM3 [11]. The casting speed was in both cases 74 mm/min, and the amount of cooling water was 45 m^3/h. The calculations were halted when about 25 minutes of casting had been simulated. At this point the calculated temperature field corresponded satisfactorily to the stationary phase of casting. In addition, a series of 2D simulations were carried out in which casting conditions and thermal properties were varied. ALSIM3 is currently restricted to solution domains with rectangular horizontal cross sections. The thickness of the cold ingot at the middle of the rolling faces (560mm) was used in the simulations.

Thermal properties

Values of density, thermal conductivity, specific heat and heat of fusion must be given as input to the model. In addition, the fraction liquid must be specified as a function of temperature. In order to preserve mass and enthalpy within the applied Lagrangian finite element formulation, a temperature independent density was prescribed. The liquidus and solidus temperature, heat of solidification and density used in the calculations are showed in Table II.

Table II. Thermal properties used in the calculations [17].

Property	Unit	AA1050	AA3003
T_{liq}	[°C]	657	654
T_{sol}	[°C]	646	643
ΔH_m	[J/kg]	397 000	397 000
ρ	[kg/m^3]	2705	2705

Thermal conductivity and specific heat are shown together with measured values for two comparable alloys and data for pure aluminium in Figure 5 and Figure 6. Due to differences in literature data, two different sets of data for the thermal conductivity

were applied for AA3003. Liquid flow and turbulence is not calculated in this work. Thermal conductivity in the liquid phase is therefore elevated to the value at the solidus temperature.

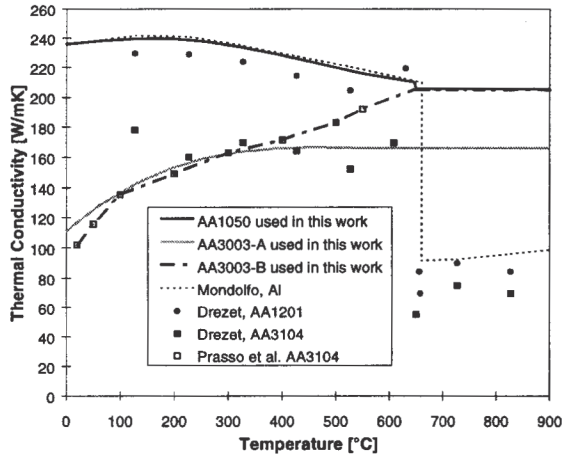

Figure 5. Thermal conductivity. The values used in this work and some literature data. [7,18,19]

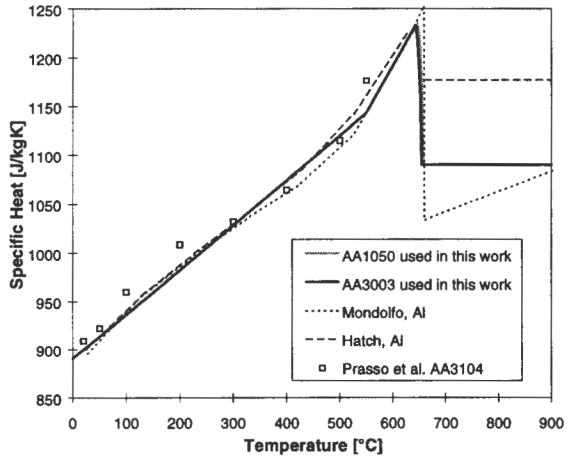

Figure 6. Specific heat. The values used in this work and some literature data. [18,19,20]

Mechanical modelling

The development of the pull-in was simulated by the 3D stress model ALSPEN3 [12,13]. This model takes as input a time sequence of temperature fields calculated in advance by the model ALSIM3. The solution domain is the part of the ingot with temperature below the coherency temperature T_c , below which the metal is considered as a solid.

2D option

ALSPEN3 may optionally be used for 2D simulations of strains and stresses in longitudinal cross sections normal to the rolling faces. Very good agreement with measurements of pull-in has been obtained by the use of a similar 2D model [9]. Using ALSPEN3, one may choose between a plain strain formulation (ε_{xx}=0) and a generalized plane strain formulation (ε_{xx}=a+bz with a and optionally b as unknowns). The generalized plane strain formulation is considered to be favorable with respect to the early start-up phase [13]. The calculated results will, however, converge to the ones from plain strain calculations as the cast length increases. As this work mainly is focused on the pull-in at stationary casting conditions, the plain strain formulation has generally been applied.

Constitutive modelling

The metal is described as an elastic-viscoplastic material and some unified constitutive equations with internal variables have been implemented in the model. A set of constitutive equations by Lalli and DeArdo [21] was applied in the simulations of castings of AA1050. For AA3003 a modified version of the MATMOD equations [22] was used (with no directional hardening).

$$\dot{\bar{\varepsilon}}^{vp} = B\Theta(T)\left\{\sinh\left[\frac{1}{a}\left(\frac{\bar{\sigma}}{d^q}\right)^{\frac{1}{1-q}}\right]\right\}^n \tag{22}$$

$$\Theta(T) = \begin{cases} \exp\left(-\dfrac{Q}{R_B T}\right) & \text{for } T \geq 0.6 \cdot T_c \\ \exp\left(\left[-\dfrac{Q}{R_B \cdot 0.6 \cdot T_c}\right]\cdot\left[\ln\left(\dfrac{0.6 \cdot T_c}{T}\right)+1\right]\right) & \text{for } T < 0.6 \cdot T_c \end{cases} \tag{23}$$

$$\dot{d} = H\dot{\bar{\varepsilon}} - HB\Theta(T)\left[\sinh\left(\frac{d}{a}\right)\right]^n \tag{24}$$

Here, $\dot{\bar{\varepsilon}}^{vp}$ is the effective viscoplastic strain rate, and R_B is the gas constant. The material constants for AA3003, see Table III, were evaluated from tensile testing[2] at temperatures ranging from 20°C to 600°C and strain rates between $2 \cdot 10^{-4}$ and $2 \cdot 10^{-2}$. d_0 is the initial value of internal variable d. Coherency temperatures of 650°C and 647°C were respectively specified for AA1050 and AA3003. There were no special handling of the mushy zone in the calculations.

Table III. Material constants for alloy AA3003

Constant	Unit	Value	Constant	Unit	Value
a	[MPa]	18.34	H	[MPa]	1750
B	[s^{-1}]	$1.435 \cdot 10^{11}$	q		0.42
n		6.414	d_0	[MPa]	0.1
Q	[kJ/mol]	217			

Numerical results and discussion

Comparison with measurements

The calculated values of pull-in were estimated from the calculated displacements $u_y(z)$, the velocities $v_y(z)$ and the mean temperature $\bar{T}(z_0)$ at a position z_0 near the bottom of the ingot at the end of numerical simulations. Based on the assumptions that both the velocity field and the temperature field have become stationary, the pull-in of the cold ingot $-u_y^e(z)$ was estimated by:

$$-u_y^e(z) = -u_y(z) - \frac{1}{V}\int_z^{z_0} v_y(z^*)\,dz^* + \beta\left(\bar{T}(z_0) - 20\right)\frac{D}{2} \tag{25}$$

[2] The experiments and the determination of the constants were carried out by SINTEF Materials Technology, Oslo, Norway.

This procedure has been validated by 2D simulations including the end phase of casting and the following cooling period. Values of pull-in measured [6] at different distances from the centre of the rolling face are shown in Figure 7 together with calculated values. A generally good agreement between measurements and 3D simulations is obtained, especially for AA3003-B thermal data. The discrepancies seen for AA1050 call for some further investigations.

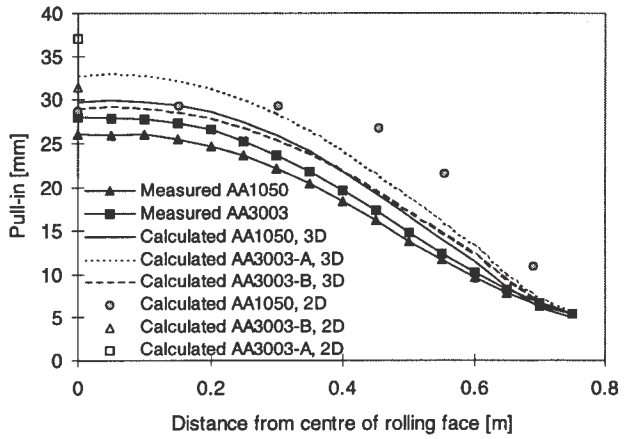

Figure 7: Calculated values of pull-in compared with measurements for the alloys AA1050 and AA3003.

Comparison with 2D results

The 3D calculations in this work required about 3–7 days of CPU time on a workstation. Comparable 2D simulations were carried out about 500 times faster. Such 2D simulations are therefore preferable, given that reliable results can be obtained.

Calculated values of pull-in from a series of 2D calculations for the alloy AA1050, based on temperature fields in cross sections at different distances from the centre of the rolling faces, are shown in Figure 7. Near the centre of the rolling face, the results from 2D calculations are in close agreement with those from 3D calculations. Large discrepancies are however seen for cross sections closer to the narrow ingot side. Evidently, some 3D effects make the applied plane strain approximation invalid in this part of the ingot. Although the pull-in at the centre of the rolling face for AA1050 is seen to be quite similar in 2D and 3D calculations, the stresses are notably different. The plain strain approximation induce large tensile forces normal to the 2D solution domain.

For AA3003 the calculated pull-in at the centre of the rolling face is significantly larger in 2D than in 3D simulations. Some interaction between the exaggerated tensile stresses induced by the plain strain assumption and stresses induced by the large temperature dependency of the thermal conductivity (giving a more non-linear variation with y of the thermal contraction rate) may possibly explain this difference.

The effect of thermal and thermomechanical data

According to the analytically derived expressions the relative pull-in is closely related to the Peclet number, but when the measured values of pull-in for ingots of different alloys are compared [6,8] it turns out that ingots of pure alloys obtain relatively more pull-in for a given Peclet number than ingots containing larger amounts of alloying elements. However, the diffusivity of pure aluminium has been reported to decrease slightly with temperature, whereas the diffusivity of more highly alloyed aluminium increases with temperature [23]. In order to investigate the effect on the pull-in of thermal and thermomechanical properties, several 2D numerical simulations were carried out. The values of density and heat capacity of AA1050 were generally applied. The values of thermal conductivity were modified in order to obtain the four different relations between temperature and thermal diffusivity shown in Figure 8. In an attempt to isolate the effect of the slope of the temperature/thermal diffusivity curve from the effect of the level of thermal diffusivity, the sump depth or the Peclet number was kept at a constant value in the series of simulations. This was achieved by changing the casting speed. In the first series the sump depth was kept constant equal to 0.664m, and the mechanical constitutive model for AA3003 was applied. In the second and third series the Peclet number was kept constant at a value of 10, and the mechanical constitutive models for AA3003 and AA1050 were applied respectively. The Peclet numbers in case A and C were based on a value of the thermal diffusivity corresponding to the average value within the interval between the liquidus temperature and 100°C. The amount of cooling water given as input to the simulations was proportional to the casting speed. As can be seen from Figure 9, the temperature dependence of the thermal diffusivity has a great influence on the pull-in.

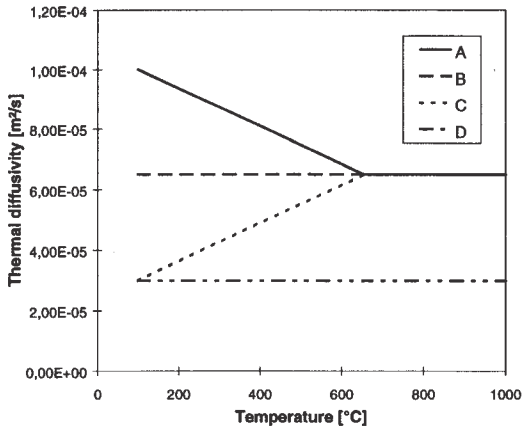

Figure 8. Diffusivity versus temperature used in the case study.

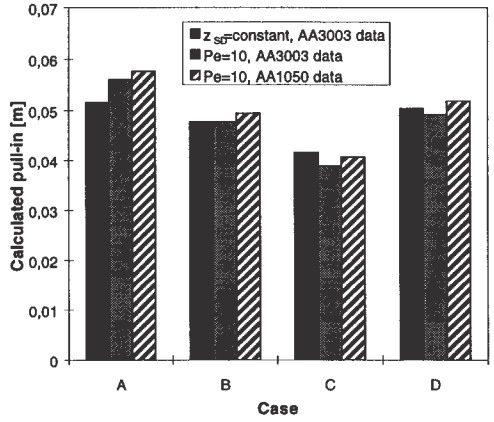

Figure 9. Pull-in calculated by use of the four different thermal diffusivity characteristics shown in Figure 8.

The value of calculated pull-in is more than 20% higher for case A than for case C, when the sump-depth is kept constant. The differences are even larger in the simulation series with constant Peclet number. This is due to some influence on the sump depth by the temperature dependence of diffusivity for constant Peclet number. The calculated pull-in for case B and D are very similar. This indicates that the level of diffusivity does not influence pull-in significantly, provided the Peclet number, or the sump depth, is kept constant. The calculated values of pull-in were, in general, 3–6% higher when the constitutive model for AA1050 was used rather than that for AA3003. We relate this to the observation that in our calculations, the ratio of flow stress at low temperatures to flow stress at high temperatures is higher for AA1050 than for AA3003. Our calculation results indicate that the effect on pull-in of different levels of thermal diffusivity may be outweighed by the effect of different slopes of the diffusivity/ temperature curve. This can to a large extent explain the observed similarity of measured values of pull-in for ingots of different alloys (for a given dimension and casting speed).

The effect of cooling conditions

In another case study, the amount of cooling water had no significant impact on the calculated pull-in, even if the sump depth was reduced by about 4%. A possible explanation is that the effect of a smaller sump depth is compensated for by larger horizontal thermal gradients due to a lower surface temperature. The use of a constant heat transfer coefficient of 10000 W/m^2K in the water cooling zone, corresponding to a relatively weak cooling effect, resulted in a calculated pull-in about 5% lower than the value obtained by simulation of normal water cooling.

Comparison with analytic expressions

A series of 2D simulations was carried out in order to validate that the approximative analytical expressions, eq. (14)–(21), account for the most essential effects related to the pull-in phenomenon. In Figure 10 we show analytically and numerically derived developments of the pull-in, at the centre of the rolling face, of an AA1050 ingot at stationary casting conditions. The corresponding horizontal velocities at the surface (or rates of pull-in) are also shown. A very good agreement is obtained. As seen in the figure, the major part of the pull-in takes place above the bottom of the sump. However, according to the interpretation of the different terms in eq. (21), the pull-in at normal casting conditions is caused mainly by thermal contractions and deformations in regions below. This has also been verified numerically. Values of relative pull-in, calculated in 2D simulations for different Peclet numbers, are compared with the approximative analytical solution (21) and literature data in Figure 11. Again, a very good agreement is obtained. The analytically predicted transition to a more quadratic dependency for very large Peclet numbers is reproduced by the simulations. According to eq. (18), the relative importance of the deformation mode II, illustrated in Figure 3, increase with the Pe number. This mode involves a horizontal contraction, whereas the zz-component of the (viscoplastic) strain rate must compensate for the axial thermal contractions. This is in accordance with the differences between the contour plots seen in Figure 12, in which the zz-components of the viscoplastic strain rate, as obtained from 2D simulations with Peclet numbers of 5 and 15 respectively, are compared.

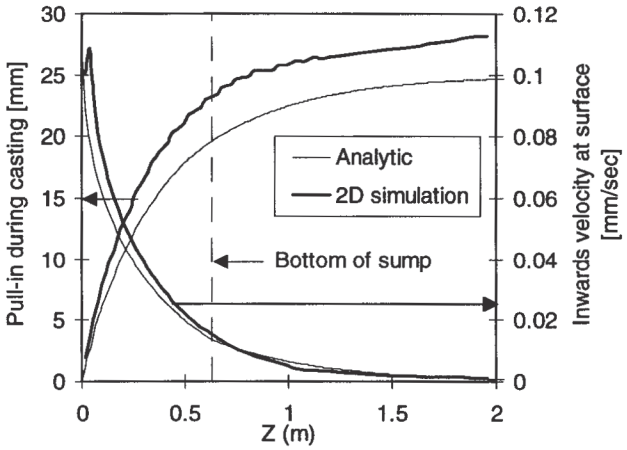

Figure 10: Pull-in and velocity at surface during casting of AA1050 derived analytically, eq. (14)–(20), and numerically by a 2D simulation.

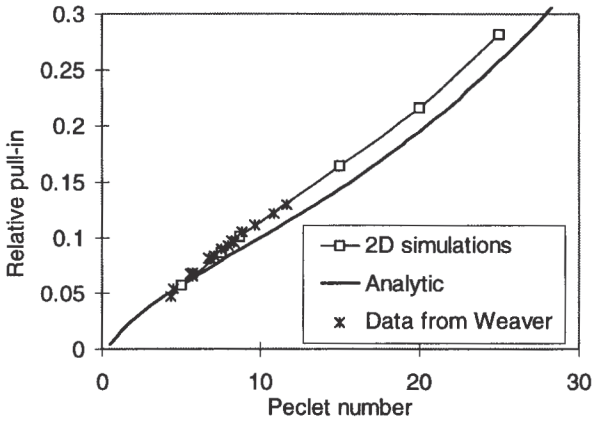

Figure 11. Calculated relative pull-in for different Peclet numbers compared with measurements [1] and approximative analytic solution.

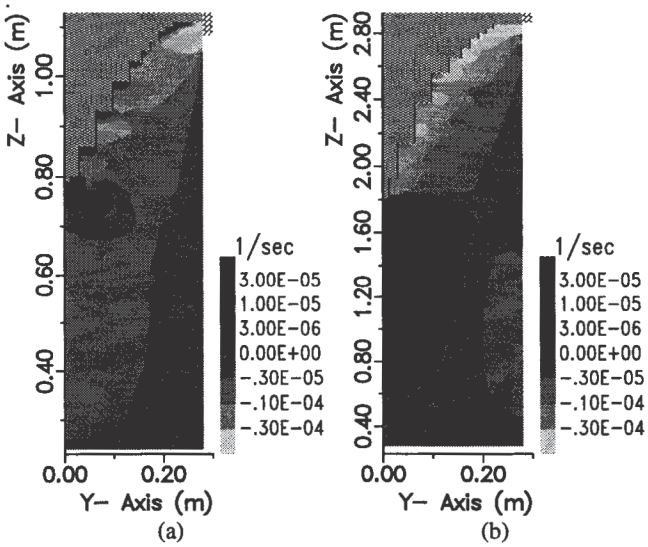

Figure 12: zz-component of viscoplastic strain rate from 2D simulations with (a) Pe=5 and (b) Pe=15. In (b) the Z-axis (here positive direction upwards) has been compressed by a factor 3.

Concluding remarks

The observed simple linear relationship between the pull-in and the casting speed for a given alloy and ingot dimension has been found to have a rather complex explanation. In an approximative analytical solution the contribution to the pull-in associated with the thermal contraction in the solid regions above the bottom of the sump increases quadratically with the casting speed, whereas the contribution from thermally induced deformations in the regions below the sump level off to some limit value at high casting speeds.

The fact that the pull-in is nearly independent of alloy composition, even if different alloys have quite different thermal and mechanical properties, may possibly be explained by the strong effect on the pull-in, seen in numerical simulations, of the temperature dependency of the thermal diffusivity. Numerical results also indicate that the mechanical constitutive behavior do have some influence. This emphasizes the need for more accurate determination of thermal and mechanical properties for industrial alloys.

Acknowledgements

This work has been funded by Hydro Aluminium. The development of the models ALSIM3 and ALSPEN3 has been funded by Hydro Aluminium, Elkem Aluminium and The Research Council of Norway.

References

1. C. H. Weaver, "An empirical model to explain cross-section changes of D.C. sheet ingot during casting," in Light Metals, TMS-AIME, (1976), 441–456.

2. C. Weaver et al, "Designing sheet ingot moulds to produce rectangular ingots of desired thickness and width," Light Metals, TMS, (1991), 953–959.

3. H. Yu, "A process to reduce DC ingot butt curl and swell," Light Metals, TMS-AIME, (1980), 613–628.

4. R. R. Lawrence. "Cross-section shape control of D.C. sheet ingot using a flexible mould," Light Metals, TMS-AIME, (1976), 457–463.

5. W. Schneider and E. K. Jensen, "Development of a new starting block shape for the D. C. Casting of sheet ingots. Part I: Experimental Results," Light Metals, TMS, (1995), 961–967.

6. A. Håkonsen, "A model to predict the stationary pull-in during DC-casting of aluminium sheet ingots", Light Metals, TMS, (1997), (this volume).

7. J.-M. Drezet, "Direct Chill and Electromagnetic Casting of Aluminium Alloys: Thermomechanical effects and solidifation aspects," (PhD thesis, EPFL, Lausanne, 1996).

8. J.-M. Drezet and M. Plata, "Thermomechanical effects during direct chill and electromagnetic casting of aluminium alloys. Part I: experimental results," Light Metals, TMS, (1995), 931–940.

9. J.-M. Drezet and M. Rappaz and Y. Krahenbuhl, "Thermomechanical effects during direct chill and electromagnetic casting of aluminium alloys. Part II: Numerical simulations," Light Metals, TMS, (1995), 941–950.

10. J.-M. Drezet, M. Rappaz, B. Carrupt, and M. Plata, "Experimental investigation of thermomecanical effects during direct chill and electromagnetic casting of aluminium alloys," Metallurgical Transactions, 26B (1995), 821–829.

11. A. Håkonsen and D. Mortensen, "A FEM model for the calculation of heat and fluid flows in DC casting of aluminium slabs," Modeling of Casting, Welding and Advanced Solidification Processes VII., TMS, (1995), 963–970.

12. H. G. Fjær and E. K. Jensen, "Mathematical modelling of butt curl deformation of sheet ingots. Comparison with experimental results for different starting block shapes", Light Metals, TMS (1995) 951–959.

13. H. G. Fjær and E. K. Jensen, "Mathematical modelling of butt curl deformation of DC cast sheet ingots. influence of starting block shape and starting conditions", Stranggießen, DGM, (1995). 951–959.

14. A. Håkonsen and O. R. Myhr, "Dimensionless diagrams for the temperature distribution in direct-chill continous casting", Cast Metals, 8 (3) (1995), 147–157.

15. J. Crank, Free and moving boundary problems, (Oxford University Press 1984).

16. B. W. Char et al., Maple V Language Reference Manual, (Springer-Verlag, 1991).

17. ASM Handbook. Vol. 2. (1990).

18. L. F. Mondolfo, Aluminium Alloys: Structure and Properties, (Butterworths, Boston, 1976,) 56-67.

19. D. C. Prasso, J. W. Evans and I. J. Wilson, "Heat Transport and Solidification in the Electromagnetic Casting of Aluminium Alloys: Part II. Development of a Mathematical Model and Comparison with Experimental results," Metallurgical Transactions, 26B (1994), 1281–1288

20. J. E. Hatch, ed. Aluminium Properties and Physical Metallurgy, (ASM, Metals Park, Ohio, 1983).

21. L. A. Lalli and A. J. DeArdo, "Experimental assessment of structure and property predictions during hot working," Metallurgical Transactions, 21A (1990), 3101–3113.

22. A. K. Miller, "A unified phenomenological model for the monotonic, cyclic, and creep deformation of strongly work-hardening materials," (PhD thesis, Stanford University, 1975).

23. C. Y. Ho et al., "Thermal Conductivity of Ten Selected Binary Alloy Systems", Journal of Physics and Chemistry Data, 7(3) (1978) 959-1176.